Neural Networks 99 (2018) 92–100

Contents lists available at ScienceDirect

Neural Networks

journal homepage: www.elsevier.com/locate/neunet

An optimal control strategy for hybrid actuator systems: Application to an artificial muscle with electric motor assist

Koji Ishihara *, Jun Morimoto

Department of Brain Robot Interface, ATR Computational Neuroscience Laboratories, Kyoto, 619-0288, Japan
Graduate School of Information Science, Nara Institute of Science and Technology, Nara, 630-0192, Japan

ARTICLE INFO

Article history:
Received 20 May 2017
Received in revised form 14 November 2017
Accepted 19 December 2017
Available online 11 January 2018

Keywords:
Motor control
Optimal control
Model predictive control
Hybrid actuator system

ABSTRACT

Humans use multiple muscles to generate such joint movements as an elbow motion. With multiple lightweight and compliant actuators, joint movements can also be efficiently generated. Similarly, robots can use multiple actuators to efficiently generate a one degree of freedom movement. For this movement, the desired joint torque must be properly distributed to each actuator. One approach to cope with this torque distribution problem is an optimal control method. However, solving the optimal control problem at each control time step has not been deemed a practical approach due to its large computational burden. In this paper, we propose a computationally efficient method to derive an optimal control strategy for a hybrid actuation system composed of multiple actuators, where each actuator has different dynamical properties. We investigated a singularly perturbed system of the hybrid actuator model that subdivided the original large-scale control problem into smaller subproblems so that the optimal control outputs for each actuator can be derived at each control time step and applied our proposed method to our pneumatic–electric hybrid actuator system. Our method derived a torque distribution strategy for the hybrid actuator by dealing with the difficulty of solving real-time optimal control problems.

1. Introduction

Although robotics technologies have rapidly improved and are widely used in industry and daily life, it remains difficult for robots to generate human-like flexible movements to work in cluttered environments (Defense Advanced Research Projects Agency, 2015) or to assist human behaviors (Ansari, Atkeson, Choset, & Travers, 2015). One reason that deters the development of such robot systems is that robots lack a light, compliant but strong actuator that works like the human muscles. As a matter of practice, electric motors with high reduction gears, which are dominantly used as robot actuators, tend to be heavy and rigid for generating large torques. Although such muscle-like actuators as a pneumatic artificial muscle (PAM) have similar properties to human muscles, control latency due to the air flow is inevitable since PAM uses air pressure to generate joint torque. Therefore, PAM has not been widely used in robot systems.

On the other hand, humans use multiple muscles to efficiently generate a joint movement. For example, at least the biceps and triceps are involved in the one degree of freedom of an elbow joint movement. In the biceps, there are two different bundles: biceps long head and biceps short head. The triceps has three different bundles: triceps long head, triceps lateral head, and triceps medial head (Burdet, Franklin, & Milner, 2013). Similarly, from a technical point of view, robots might be able to use multiple actuators to generate a joint motion. To explore this possibility, hybrid actuation systems have been developed and implemented in robot systems (Hyon, Morimoto, Matsubara, Noda, & Kawato, 2011; Noda, Teramae, Ugurlu, & Morimoto, 2014; Sardellitti, Park, Shin, & Khatib, 2007). However, how to distribute the desired torque to each actuator has not been scrutinized. One possible approach to cope with this torque distribution problem is using an optimal control method (Matsubara, Noda, Hyon, & Morimoto, 2011; Teramae, Noda, & Morimoto, 2014). The optimal control framework provides a powerful tool for robot motion generation in a diverse set of tasks and applications to actuator control (Braun, Howard, & Vijayakumar, 2012; Haddadin, Weis, Wolf, & Albu-Schäffer, 2011) since optimal motor commands can be derived under the constraint of their own dynamics by specifying simple high-level task goals. However, solving an optimal control problem at each control time step has not been considered as a practical approach due to the large computational burden.

In this paper, we propose a computationally efficient method to derive an optimal control strategy for a hybrid actuation system composed of multiple actuators, where each actuator has different

* Correspondence to: Department of Brain Robot Interface, ATR Computational Neuroscience Laboratories, 2-2-2, Hikaridai Seika-cho Soraku-gun, Kyoto, 619-0288, Japan.
E-mail addresses: ishihara-k@atr.jp (K. Ishihara), xmorimo@atr.jp (J. Morimoto).

https://doi.org/10.1016/j.neunet.2017.12.010

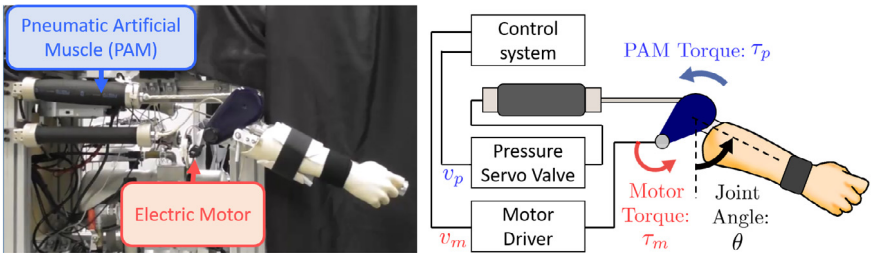

Fig. 1. Forearm robot with pneumatic–electric hybrid actuator system: pneumatic artificial muscle dominantly generates torques but is assisted by small and lightweight electric motor for precise movements. v_p denotes voltage input for air valve, and v_m denotes voltage input for motor driver. We used one pneumatic artificial muscle and one electric motor.

dynamical properties. We derive a new singularly perturbed system of hybrid actuator dynamics to subdivide the original control problem into smaller subproblems so that the optimal control outputs for each actuator can be derived at each control time step. The singularly perturbed system has been intensively studied to describe fluid dynamics (Lagerstrom & Casten, 1972; Van Dyke, 1975), which shows different properties in the regions close and far from the wall due to its viscosity. Inspired by these kinds of studies, it was found that even robot systems, which have particular dynamic properties such as a biped robot or a flexible robot manipulator, can be represented as singularly perturbed systems (Arimoto & Miyazaki, 1980; Siciliano & Book, 1988).

A method that derives optimal control outputs at each control time step is known as Model Predictive Control (MPC). MPC methods have been applied to such slow dynamical systems as chemical plants (Qin & Badgwell, 1997) or ship maneuvering problems (Seguchi & Ohtsuka, 2003) since a sufficient amount of time for calculating the computationally intensive optimal control problem can be used in slowly responding systems. However, directly applying MPC to the real-time control of such faster dynamics as robot systems is unrealistic. In this study, we newly derived singular perturbed system for a hybrid actuator and applied MPC to the subdivided control problems. Based on an idea of using MPC for a simulated system that includes different time scale dynamics (Chen, Heidarinejad, Liu, & Christofides, 2012; Ishihara & Morimoto, 2015), we developed a two-stage MPC framework for the hybrid actuation system and showed that our proposed method was able to successfully control the real robot. Both optimization stages correspond to either the extracted fast components of the singularly perturbed system or the original dynamics that include a slow dynamical component. Then for the fast dynamical component, we propose short-term optimization with fine-control time resolution. Since a robot can quickly change its behavior with the fast dynamical component, the long-term optimization is not necessary. Instead, we can utilize computational resources to generate precise movements with higher time resolution. On the other hand, for the original dynamics, we address long-term optimization with coarse-time resolution. Since a robot cannot quickly change its behavior with the original dynamics that includes the slow dynamical component, we need to consider the long-term optimization problem. However, for the original dynamics, we can use the optimization problem with lower time resolution that requires less computation since we can rely on the optimization of the fast dynamical component to generate movements for fine-time resolution.

To evaluate the torque distribution performance of our proposed approach, we applied the two-stage optimization procedure to our pneumatic–electric hybrid actuator system, where PAM dominantly generates joint torques but is assisted by a small and lightweight electric motor for precise movements (Fig. 1). We first derived a singularly perturbed system for the hybrid actuation system based on the difference of the dynamic properties between

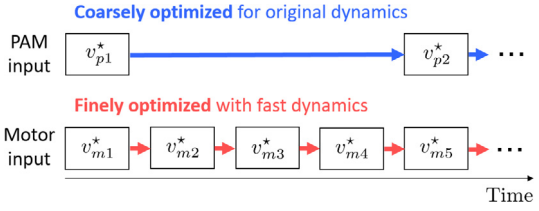

Fig. 2. Two-stage optimization strategy: Each thread corresponds to either fast component of singularly perturbed system or original system. For fast dynamical component, we propose short-term optimization with fine-control time resolution. Since a robot can quickly change its behavior with fast dynamical component, long-term optimization problem is not necessary and we utilize computational resources to generate precise movements with higher time resolution. For original dynamics, we address long-term optimization with coarse-time resolution. Since a robot cannot quickly change its behavior with original dynamics that includes slow dynamical component, we need to consider long-term optimization problem. However, in two-stage optimization strategy, we can use optimization problem with lower time resolution that requires less computation since we can rely on optimization of fast dynamical component to generate movements for fine-time resolution. v_p denotes voltage input for air valve, and v_m denotes voltage input for motor driver.

PAM and the electric motor. From this theoretical analysis, we found that only the lower-dimensional subspace of the original system needs to be considered in the fast dynamical component and that only the electric motor outputs affect the behavior of the lower-dimensional subspace. Our method properly derived a torque distribution strategy for the hybrid actuation system by solving a real-time optimal control problem and successfully reduced the computation time without significantly deteriorating the control performance. In the proposed approach, after deriving the optimal input voltages for the air valve and the motor driver with coarse-time resolution, only the optimal sequence of the input voltage for the motor driver was further optimized with fine-time resolution under the lower-dimensional dynamics (see Fig. 2). For a comparison, we also applied two standard implementations of the MPC method with two different time resolutions each: optimal control strategies with fine-time resolution and coarse-time resolution to our hybrid actuator system. The coarse strategy corresponds to the optimization process for the original dynamics of our proposed method. Therefore, we can evaluate the effectiveness of the optimization for the fast dynamics component by comparing the tracking results of the coarse strategy and our proposed approaches. To the best of our knowledge, for the first time in the literature, a real robot with a hybrid actuator system is proposed as a singularly perturbed system and is successfully controlled in real-time with the new two-stage optimal control method.

The rest of our paper is organized as follows. Section 2 explains a standard MPC problem. Section 3 introduces our proposed two-stage optimal control method. Section 4 describes about the tasks, their goals and experimental setting. Section 5 shows the experimental results .

2. Model predictive control

In MPC at each control period, a finite-horizon optimal control problem is solved to find an optimal control sequence that minimizes the accumulated cost over a finite future horizon. We evaluate the objective function based on a state trajectory and a control sequence estimated using a nonlinear system model:

$$\mathbf{x}_{k+1} = \mathbf{f}_{\Delta t}(\mathbf{x}_k, \mathbf{u}_k), \tag{1}$$

where $\mathbf{x} \in \mathbb{R}^n$ and $\mathbf{u} \in \mathbb{R}^m$ respectively denote the state vectors and control inputs. Δt denotes a control period. The accumulated cost is defined as

$$J(\mathbf{x}_k, \mathbf{U}_k) = \sum_{i=k}^{k+N-2} l(\mathbf{x}_i, \mathbf{u}_i) + l_T(\mathbf{x}_{k+N-1}), \tag{2}$$

where $\mathbf{U}_k \equiv \{\mathbf{u}_k, \mathbf{u}_{k+1}, \ldots, \mathbf{u}_{k+N-2}\}$ is the control sequence. $l(\mathbf{x}, \mathbf{u})$ is the immediate cost and $l_T(\mathbf{x})$ is the terminal cost.

The optimal control sequence is defined as:

$$\mathbf{U}_k^\star \equiv \arg\min_{\mathbf{U}_k} J(\mathbf{x}_k, \mathbf{U}_k), \tag{3}$$

where * indicates optimized variables. Once the optimal control sequence $\mathbf{U}_k^\star$ is derived, the first few elements (usually only first element $\mathbf{u}_k^\star$) of the optimal control sequence are applied to the robot. Since the optimal control sequence is computed at each time step based on the robot's current state and the current definition of the cost function, MPC can cope with external disturbances and adaptively derive control policies even with dynamically changing cost functions. To derive a locally optimal controller, we use a Differential Dynamic Programming (DDP) (Jacobson, 1968) approach called iterative Linear Quadratic Gaussian (iLQG) (Todorov & Li, 2005).

3. Proposed method

3.1. Two-stage optimal control approach

If a robot needs to generate fast movements in a real environment, the above finite optimal control problem must be solved in a short period of time.

In this study, we adopted a two-stage optimal control approach where each optimization stage corresponds to either a fast component of a singularly perturbed system or the original dynamics. Then for the fast dynamical component, we used a short-term optimization with fine-control time resolution. Since a robot can quickly change its behavior with the fast dynamical component, we can disregard the long-term optimization problem and utilize computational resources to generate precise movements with fine-time resolution. On the other hand, for the original dynamics, we address long-term optimization with coarse-time resolution. Since a robot cannot quickly change its behavior with the original dynamics that includes slow dynamical component, we need to consider the long-term optimization problem. However, for the original dynamics, we can use the optimization problem with lower time resolution that requires less computation since we can rely on the optimization of the fast dynamical component to generate movements with fine-time resolution.

MPC's computation time depends on prediction length N, the dimensionality of state space n, and dimensionality of control input m. We thus divide the original control problem into two smaller problems in terms of the prediction horizon and the state and input dimensions.

The first problem is a coarse optimization given objective function J^c and the original system dynamics:

$$\min_{\tilde{\mathbf{U}}_k} J_k^c(\tilde{\mathbf{x}}_k, \tilde{\mathbf{U}}_k) \tag{4a}$$

$$\text{s.t. } \tilde{\mathbf{x}}_{k+1} = \mathbf{f}_{\Delta t_c}(\tilde{\mathbf{x}}_k, \tilde{\mathbf{u}}_k), \tag{4b}$$

where $\tilde{\mathbf{x}}$ and $\tilde{\mathbf{U}}_k \equiv \{\tilde{\mathbf{u}}_k, \tilde{\mathbf{u}}_{k+1}, \ldots, \tilde{\mathbf{u}}_{k+N-2}\}$ denote a state and a control sequence for the coarse optimization. Δt_c is a coarse time step ($\Delta t_c > \Delta t$).

To generate a fast movement, the coarse input sequence derived in the coarse optimization must be further optimized with a fine-time resolution. Then, the objective of fine optimization is to refine the result of the first optimization. In the second optimization, we use shorter time step Δt_f rather than coarse time step Δt_c. Horizon for the fine optimization is defined as N_f. The second optimization problem is smaller than the original one in terms of input and state dimensions since a reduced-order subsystem is only considered as the constraints.

We extracted a fast subsystem from the original system dynamics based on a singularly perturbed system. The detailed process to extract a fast dynamics of the hybrid actuator system is described in Section 3.2. Optimal control methods for singularly perturbed systems have been studied (Kokotovic, Khalil, & O'reilly, 1999; Naidu, 2002). A singularly perturbed system in standard form is represented below:

$$\begin{aligned} \dot{\mathbf{y}} &= \mathbf{h}(\mathbf{y}, \mathbf{z}, \mathbf{u}^{\mathbf{y}}, \mathbf{u}^{\mathbf{z}}) \\ \varepsilon \dot{\mathbf{z}} &= \mathbf{g}(\mathbf{y}, \mathbf{z}, \mathbf{u}^{\mathbf{y}}, \mathbf{u}^{\mathbf{z}}), \end{aligned} \tag{5}$$

where $\mathbf{y} \in \mathbb{R}^{n_y}$, $\mathbf{z} \in \mathbb{R}^{n_z}$, $\mathbf{u}^{\mathbf{y}} \in \mathbb{R}^{m_y}$ and $\mathbf{u}^{\mathbf{z}} \in \mathbb{R}^{m_z}$ respectively denote the vectors of slow, fast state variables, and control inputs for slow and fast states. ε is a small positive parameter. After transforming the original system dynamics into a singularly perturbed system, we extract a fast subsystem from it.

We, first, convert the optimal state and input trajectories derived in coarse optimization. We transform the optimal trajectories described in the original state and action space into ones described in the slow and fast state–action space: from the trajectories of $\tilde{\mathbf{x}}^\star$ and $\tilde{\mathbf{u}}^\star$ into the trajectories of $\tilde{\mathbf{y}}^\star$, $\tilde{\mathbf{z}}^\star$, $\tilde{\mathbf{u}}^{\mathbf{y}^\star}$ and $\tilde{\mathbf{u}}^{\mathbf{z}^\star}$. Then, we use zero-order hold model to keep optimized states and control inputs for $M = \Delta t_c / \Delta t_f$ time steps to match up the optimal trajectories with the time scale of the fast subsystem:

$$\begin{aligned} [\hat{\mathbf{y}}_j^\star, \hat{\mathbf{y}}_{j+1}^\star, \ldots, \hat{\mathbf{y}}_{j+M-1}^\star] &\leftarrow [\tilde{\mathbf{y}}_k^\star, \tilde{\mathbf{y}}_k^\star, \ldots, \tilde{\mathbf{y}}_k^\star] \\ [\hat{\mathbf{z}}_j^\star, \hat{\mathbf{z}}_{j+1}^\star, \ldots, \hat{\mathbf{z}}_{j+M-1}^\star] &\leftarrow [\tilde{\mathbf{z}}_k^\star, \tilde{\mathbf{z}}_k^\star, \ldots, \tilde{\mathbf{z}}_k^\star] \\ [\hat{\mathbf{u}}_j^{\mathbf{y}^\star}, \hat{\mathbf{u}}_{j+1}^{\mathbf{y}^\star}, \ldots, \hat{\mathbf{u}}_{j+M-1}^{\mathbf{y}^\star}] &\leftarrow [\tilde{\mathbf{u}}_k^{\mathbf{y}^\star}, \tilde{\mathbf{u}}_k^{\mathbf{y}^\star}, \ldots, \tilde{\mathbf{u}}_k^{\mathbf{y}^\star}] \\ [\hat{\mathbf{u}}_j^{\mathbf{z}^\star}, \hat{\mathbf{u}}_{j+1}^{\mathbf{z}^\star}, \ldots, \hat{\mathbf{u}}_{j+M-1}^{\mathbf{z}^\star}] &\leftarrow [\tilde{\mathbf{u}}_k^{\mathbf{z}^\star}, \tilde{\mathbf{u}}_k^{\mathbf{z}^\star}, \ldots, \tilde{\mathbf{u}}_k^{\mathbf{z}^\star}] \end{aligned} \tag{6}$$

where the subscript $j = (k-1)M + 1$ indicates the time index of fine-time resolution and k denotes the time index of the coarse-time resolution.

Let us define the deviation of a fast state from the optimal fast state in the first optimization as $\boldsymbol{\zeta} = \mathbf{z} - \hat{\mathbf{z}}^\star$, the control input difference as $\boldsymbol{\nu} = \mathbf{u}^{\mathbf{z}} - \hat{\mathbf{u}}^{\mathbf{z}^\star}$, and a sequence of the deviations of control inputs as $\mathbf{N}_j \equiv \{\boldsymbol{\nu}_j, \boldsymbol{\nu}_{j+1}, \ldots, \boldsymbol{\nu}_{j+N_f-2}\}$, and formulate the fine optimization problem to modify the result of the first optimization:

$$\min_{\mathbf{N}_j} J_j^f(\hat{\mathbf{Y}}^\star, \hat{\mathbf{Z}}^\star, \hat{\mathbf{U}}^{\mathbf{y}^\star}, \boldsymbol{\zeta}_j, \mathbf{N}_j) \tag{7a}$$

$$\text{s.t. } \boldsymbol{\zeta}_{k+1} = \hat{\mathbf{g}}_{\Delta t_f}(\hat{\mathbf{y}}_j^\star, \hat{\mathbf{u}}_j^{\mathbf{y}^\star}, \boldsymbol{\zeta}_j, \boldsymbol{\nu}_j, \varepsilon), \tag{7b}$$

where

$$\begin{aligned}\hat{\mathbf{Y}}^\star &\equiv \{\hat{\mathbf{y}}_j^\star, \hat{\mathbf{y}}_{j+1}^\star, \ldots, \hat{\mathbf{y}}_{j+N_f-1}^\star\}\\ \hat{\mathbf{Z}}^\star &\equiv \{\hat{\mathbf{z}}_j^\star, \hat{\mathbf{z}}_{j+1}^\star, \ldots, \hat{\mathbf{z}}_{j+N_f-1}^\star\}\\ \hat{\mathbf{U}}^{\mathbf{y}^\star} &\equiv \{\hat{\mathbf{u}}_j^{\mathbf{y}^\star}, \hat{\mathbf{u}}_{j+1}^{\mathbf{y}^\star}, \ldots, \hat{\mathbf{u}}_{j+N_f-2}^{\mathbf{y}^\star}\}\\ \hat{\mathbf{U}}^{\mathbf{z}^\star} &\equiv \{\hat{\mathbf{u}}_j^{\mathbf{z}^\star}, \hat{\mathbf{u}}_{j+1}^{\mathbf{z}^\star}, \ldots, \hat{\mathbf{u}}_{j+N_f-2}^{\mathbf{z}^\star}\}.\end{aligned} \tag{8}$$

Horizon N_f is set as $\Delta t_f N_f < \Delta t_c N$ in our evaluations because the controller for the fast subsystem modifies the robot's short-term effect. The extracted fast subsystem is shown as $\hat{\mathbf{g}}_{\Delta t_f}$ in Eq. (7b).

Finally, the control input for the fast state at time j is composed of two control variables:

$$\mathbf{u}_j^\star = \begin{bmatrix}\mathbf{u}_j^{\mathbf{y}^\star}\\ \mathbf{u}_j^{\mathbf{z}^\star}\end{bmatrix} = \begin{bmatrix}\tilde{\mathbf{u}}_j^{\mathbf{y}^\star}\\ \tilde{\mathbf{u}}_j^{\mathbf{z}^\star} + \boldsymbol{\nu}_j^\star\end{bmatrix}. \tag{9}$$

3.2. Extraction of fast dynamics

In order to apply the two-stage optimization procedure to our pneumatic–electric hybrid actuator system, we derive a singularly perturbed system for a hybrid actuator composed of a pneumatic artificial muscle and a small lightweight electric motor. By investigating the time constant of the first-order air pressure dynamics as a time scale to extract the fast dynamical component from the hybrid actuation system, we find that only the electric input affects the fast dynamical component.

The motion equations of a forearm robot with the hybrid actuator are expressed as follows:

$$\begin{aligned}T_p\dot{P} &= -k_{vp}P + v_p\\ I\ddot{\theta} &= c(\theta, \dot{\theta}) + \tau_p(P, \theta) + \tau_m(v_m),\end{aligned} \tag{10}$$

where I is the inertia and c is the vector of the total external forces, such as gravity and friction forces. The output torques generated with the pneumatic actuator and the electric motor are τ_p and τ_m, respectively. The transformation coefficient of the pressure to a voltage scale is denoted as k_{vp}. The time constant parameter of the air valve is represented as T_p.

The joint angle and angular velocity are denoted as θ and $\dot{\theta}$, P stands for the PAM pressure, and v_m and v_p are the input voltages for the electric motor and PAM. State $\mathbf{x}$ of the state–space model consists of the positions, the velocities, and the PAM pressure: $\mathbf{x} = [\theta, \dot{\theta}, P]^\top \in \mathbb{R}^3$. The input vector is composed of the input voltages: $\mathbf{u} = [v_m, v_p]^\top \in \mathbb{R}^2$. We adopted a smooth friction model (Makkar, Dixon, Sawyer, & Hu, 2005) and a second-order pneumatic actuator model (Teramae et al., 2014).

In general, the PAM pressure does not change as fast as the electrical motors since the air flow is much slower than the electrical current. Air pressure P is slower than joint angle θ and its velocity $\dot{\theta}$ is affected by the electric motor as a result of the relatively large value of time constant parameter T_p. To extract the fast dynamics, we define ε in Eq. (5) as $\varepsilon = 1/T_p$ and use the deviations of the fast states and the control input from the optimal fast ones in the coarse optimization as $\zeta_1 = \theta - \tilde{\theta}^\star$, $\zeta_2 = \dot{\theta} - \dot{\tilde{\theta}}^\star$ and $\nu = v_m - \tilde{v}_m^\star$. By rewriting Eq. (10) with the defined variables and setting $\varepsilon \to 0$, we obtain the following fast subsystem:

$$\dot{P} = 0. \tag{11a}$$

$$I\dot{\zeta}_2 = c(\zeta_1 + \tilde{\theta}^\star, \zeta_2 + \dot{\tilde{\theta}}^\star) + \tau_p(\tilde{P}^\star, \zeta_1 + \tilde{\theta}^\star) + \tau_m(\nu + \tilde{v}_m^\star). \tag{11b}$$

Eq. (11) describes the dynamics of the fast states under the fixed slow variables. Since control inputs do not only affect the slow states, the discretized reduced-order subsystem of Eq. (11b) is considered as a constraint in the fine optimization of Eq. (7).

4. Experiments

We evaluated our proposed method on our forearm robot with the hybrid actuation system (Fig. 1) in tracking control problems. For the target joint trajectories we used different sinusoidal patterns in terms of frequencies at 0.25, 0.5, and 1.0 Hz with a peak-to-peak amplitude of $\pm 30^\circ$. From the derived singularly perturbed system, we applied the two-stage optimization approach to the slow and fast dynamical components of the actuator system. We used one PAM actuator and one electric motor of our forearm robot to evaluate our proposed approach.

In this experiment, the cost function for the optimal control method was composed of four terms: error between the desired and current joint angles, penalties on the PAM pressure, control cost for joint torques due to the PAM and the electric motor outputs, and control cost for input voltages of the air valve and the motor driver. Specifically, the robot minimized the total cost of the immediate cost function ℓ accumulated along the predicted trajectory and the terminal cost function ℓ_T, where

$$\begin{aligned}\ell &= w_\theta(\theta - \theta^d)^2 + w_P \mathrm{smin}(P - P_0, 0)^2 + w_\tau(\tau_p^2 + \tau_m^2)\\ &\quad + w_v(v_p^2 + v_m^2),\end{aligned} \tag{12a}$$

and

$$\ell_T = w_\theta(\theta - \theta^d)^2 + w_P \mathrm{smin}(P - P_0, 0)^2. \tag{12b}$$

$\mathrm{smin}(a, b)$ is a smooth approximation to $\min(a, b)$. In this experiment, we utilized the following function:

$$\mathrm{smin}(a, b) = -\frac{\sqrt{(a-b)^2 + \gamma^2} - a - b}{2}, \tag{13}$$

where γ is a constant to regulate the smoothness. We used $\gamma = 0.1$ in the experiment. The target angle at a time step is denoted as θ^d. If the PAM pressure falls below P_0, the wire connecting the PAM and the robot loses its tension and the pneumatic actuator cannot generate any torque. The second term on the right-hand side in Eq. (12) is the penalty on it. In the proposed method, the same cost function is used in both stages except the control costs. In the second stage, the immediate cost includes the deviation of the fast control input instead of the input voltages. We set the each weight as $w_\theta = 40$, $w_P = 30$, $w_\tau = 0.1$, $w_v = 0.002$ and limited the domains of the control variables, as in $0 \le v_p \le 5.0$ and $-5.0 \le v_m \le 5.0$. For comparisons presented in Fig. 4, we varied the weight for the voltage input as $w_v = 0.02$, 0.002 and 0.0002. The forearm robot weighed 2.7 kg. The sampling and control periods were 4.0 [ms]. Optimal input voltage command to the air valve of the PAM and the motor driver of the small lightweight electric motor needed to be derived within the control period.

In this experiment, we also applied two standard implementations of the MPC method each to compare the results with our proposed method. In the fine optimal control strategy, the optimal control sequence Eq. (3) for a fine time step is derived while a coarse time step is used in the coarse control strategy. Table 1 shows the time steps and the horizon used in each method. To investigate the effect of the time step size for the standard MPC implementations, we varied the time step size as 4.0 ms and 8.0 ms for the fine strategies and as 20.0 ms and 40.0 ms for the coarse strategies. At each control step, we solved finite optimal control problems with a 200-ms time horizon.

All the optimal controllers presented in the study were derived through a C language programming environment on an Intel Xeon Processor E5-2697 v3, 2.6-GHz computer. The maximum number of iteration and termination criteria for iLQG were 50 and 5.0×10^{-4} respectively in all the methods. In iLQG, we computed the derivatives of the dynamics and the costs in parallel with ten computer threads using Open Multi-Processing (OpenMP) (OpenMP ARB, 0000).

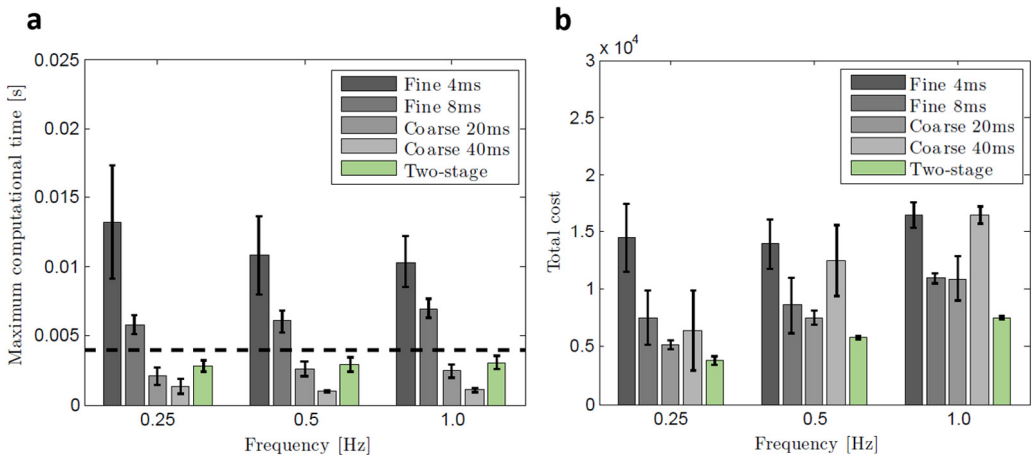

Fig. 3. Computational times and control performances: (a) maximum computation times to derive optimal control sequence for target trajectories with frequencies of 0.25, 0.5, and 1.0 Hz. We show averaged maximum computation times of five experimental trials. 4.0-ms control period is depicted by dashed black line. (b) averaged accumulated cost for 10-s duration of five tracking control trials. *Fine 4ms* strategy resulted in largest total cost for all target frequencies. *Coarse 20ms*, *40ms* and proposed two-stage strategies showed similar tracking performances for target sinusoidal trajectory of 0.25 Hz. On the other hand, for *Coarse 20ms* and *40ms* strategies, total cost increased for target trajectories with higher frequencies. Error bars represent standard deviations.

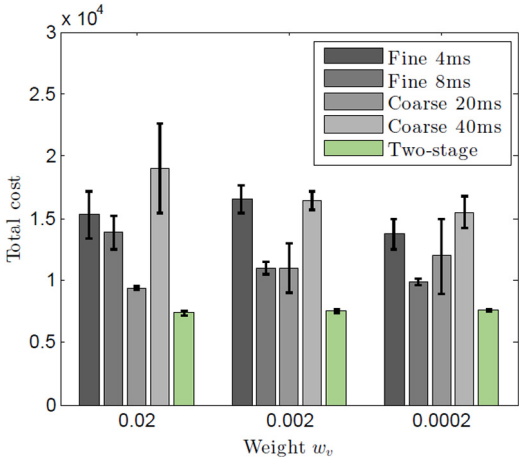

Fig. 4. Control performances with three different weights of voltage input cost: $w_v = 0.02, 0.002$ and 0.0002. Accumulated costs for 10-s duration of five tracking control trials were compared. We utilized the target trajectory with frequency of 1.0 Hz. Our proposed approach showed best control performance regardless of weight settings. Error bars represent standard deviations.

Table 1
Experimental setups of time step size and horizon length.

Method	Step size [ms]	Horizon
Fine 4ms	$\Delta t_f = 4$	$N = 50$
Fine 8ms	$\Delta t_f = 8$	$N = 25$
Coarse 20ms	$\Delta t_c = 20$	$N = 10$
Coarse 40ms	$\Delta t_c = 40$	$N = 5$
Two-stage	$\Delta t_f = 4, \Delta t_c = 20$	$N_f = 20, N = 10$

5. Results and discussion

5.1. Computational times and control performances

We first compared the fine and coarse optimal control strategies with our proposed method in terms of computational times and control performances. Fig. 3a shows the maximum computation times required to derive an optimal control sequence to track the sinusoidal target trajectories with frequencies of 0.25, 0.5, and 1.0 Hz. We showed the average maximum computation times of five experimental trials. The 4.0-ms control period is depicted by the dashed black line. Although a calculation process to derive an optimal control sequence must be terminated within 4.0 ms for real-time control, all of the maximum computational times of the fine strategies exceeded the threshold, but not the coarse and proposed strategies (Fig. 3a). These results indicate that optimal control calculation with fine-time resolution cannot be an option for the real-time control of a hybrid actuator system.

Fig. 3b shows the average accumulated cost for a 10-s duration of five tracking control trials. The accumulated cost was computed with the cost functions in Eq. (12). *Fine 4ms* strategy resulted in the largest total cost for all the target frequencies. This is mainly due to the large deviation from the target trajectory. This large deviation occurred since *Fine 4ms* strategy requires a large amount of computation time and was unable to finish the calculation within the control period. Although *Fine 8ms* strategy shows better performance than *Fine 4ms*, control outputs were not able to be derived in real time. The coarse strategies and proposed strategy showed similar tracking performance for the target sinusoidal trajectory of 0.25 Hz. On the other hand, for the coarse strategies, the total cost gradually increased for the target trajectories with higher frequencies. Although *Coarse 20ms* strategy shows the best performance in all the standard MPC implementations, our proposed approach shows even better performance than *Coarse 20ms* for all the target frequencies

Fig. 4 represents the accumulated cost for the three different weights of the voltage input cost: $w_v = 0.02, 0.002$ and 0.0002. Here, we utilized the target trajectory with frequency of 1.0 Hz. The proposed approach shows the best control performance regardless of the weight settings. The above results indicate that our two-stage optimal control framework with a newly derived singularly perturbed system successfully worked for a real hybrid actuation system.

5.2. Generated trajectories

Here, we show the generated joint angle profiles for the target sinusoidal trajectories of 0.25 and 1.0 Hz using the three different optimal control strategies in Fig. 5. We depicted the results of the proposed method with those of the worst and the best implementations of the standard MPC in terms of the comparison depicted in Fig. 3, where the worst one corresponds to *Fine 4ms* strategy and the best one corresponds to *Coarse 20ms* strategy. The target trajectories are represented by dashed orange lines. We conducted

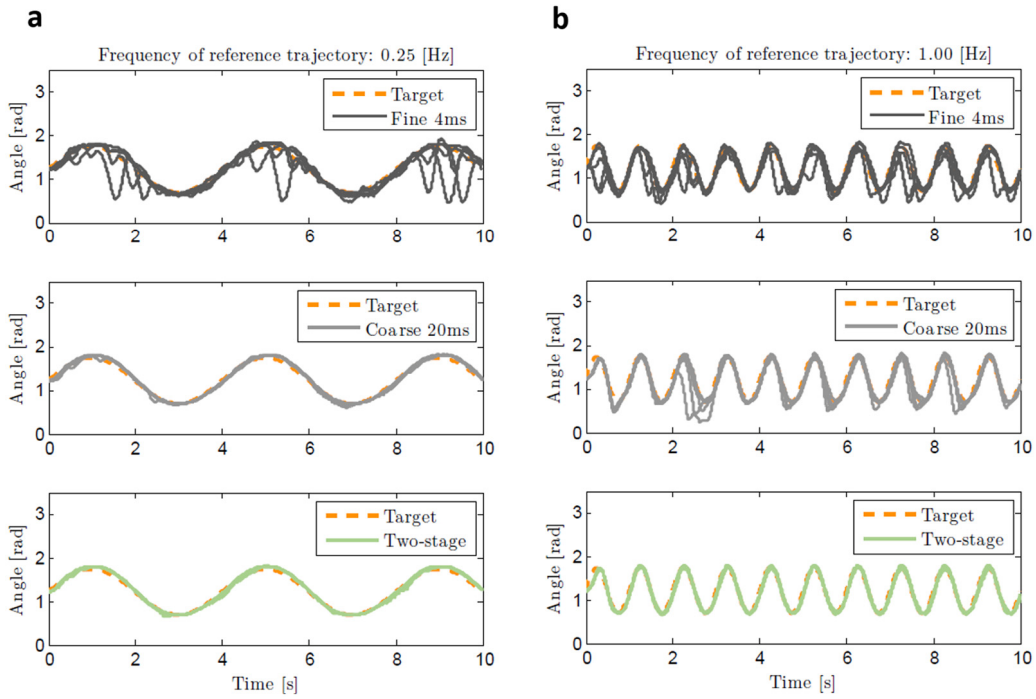

Fig. 5. Generated joint angle profiles are shown for target sinusoidal trajectories of 0.25 and 1.0 Hz using three different optimal control strategies. Target trajectories are represented by dashed orange lines. Since we conducted five experimental trials for each strategy, five trajectories are depicted for each optimal control method. (a) generated movements using the fine strategy for 0.25-Hz sinusoidal target patterns frequently deviated from target trajectory. Even with the coarse strategy, small fluctuations were observed. On the other hand, when we used our proposed strategy, generated movements consistently followed target trajectory. (b) for target trajectory with 1.0-Hz sinusoidal pattern, joint trajectories were not properly generated when we used either fine or coarse strategies. On the other hand, with proposed method, generated trajectories successfully followed target trajectory.

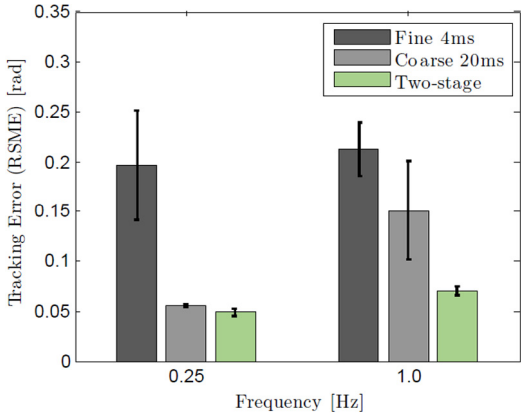

Fig. 6. Averaged tracking errors of five experimental trials each of the fine, coarse and proposed strategies. We found that our proposed approach outperformed the standard MPC implementations. Error bars represent standard deviations.

five experimental trials for each strategy and depicted the five trajectories generated using each optimal control method.

As shown in Fig. 5a, for the 0.25-Hz sinusoidal target pattern, the generated movements using the fine strategy frequently deviated from the target trajectory. Even with the coarse strategy, small fluctuations were observed. On the other hand, with our proposed strategy, the generated movements consistently followed the target trajectory. For the target trajectory with a 1.0-Hz sinusoidal pattern, the joint trajectories were not properly generated when we used either the fine or the coarse strategies (Fig. 5b).

We quantitatively compared the tracking errors of the three MPC approaches both for 0.25-Hz and 1.0-Hz sinusoidal target movements in Fig. 6. We again found that our proposed approach outperformed the standard MPC implementations.

Fig. 7 shows the generated motions of our forearm robot for the 1.0-Hz target trajectory using the three optimal control strategies. The target trajectories are depicted by dashed orange lines. For the fine and coarse strategies, the generated joint motions significantly deviated from the target movements and failed to recover from failure situations after the large deviations (Fig. 7). The motions generated by the proposed method successfully followed the target trajectory without any large tracking errors.

The above results again clearly showed the advantage of using our two-stage optimal control strategy based on the singular perturbation method. Although we evaluated our approach on the 0.25-, 0.5- and 1.0-Hz sinusoidal trajectories, similar tracking performances were observed up to a target trajectory with 1.8-Hz frequency.

5.3. Torque distributions

In the previous sections, we evaluated the control performances of our proposed optimal control strategy. Here, we show how it distributed the commanded torque to the PAM and the electric motor for precise target trajectory tracking by our proposed method. Fig. 8a shows the contributions of each actuator to generate the joint torques. We showed the average distributions of five experimental trials. Error bars represent standard deviations. Our results indicate that the contribution of the electric motor was much smaller than that of the PAM in terms of the amount of generated torque.

We then compared the tracking performance of our proposed hybrid control strategy with that of the control approach, which only uses PAM on joint trajectory tracking tasks. For PAM control, we simply used the coarse optimal control method with the settings of *Coarse 20ms* strategy in Table 1, which is equivalent to the optimization procedure for the original dynamics in our two-stage optimization method. Fig. 8b shows the averaged tracking errors

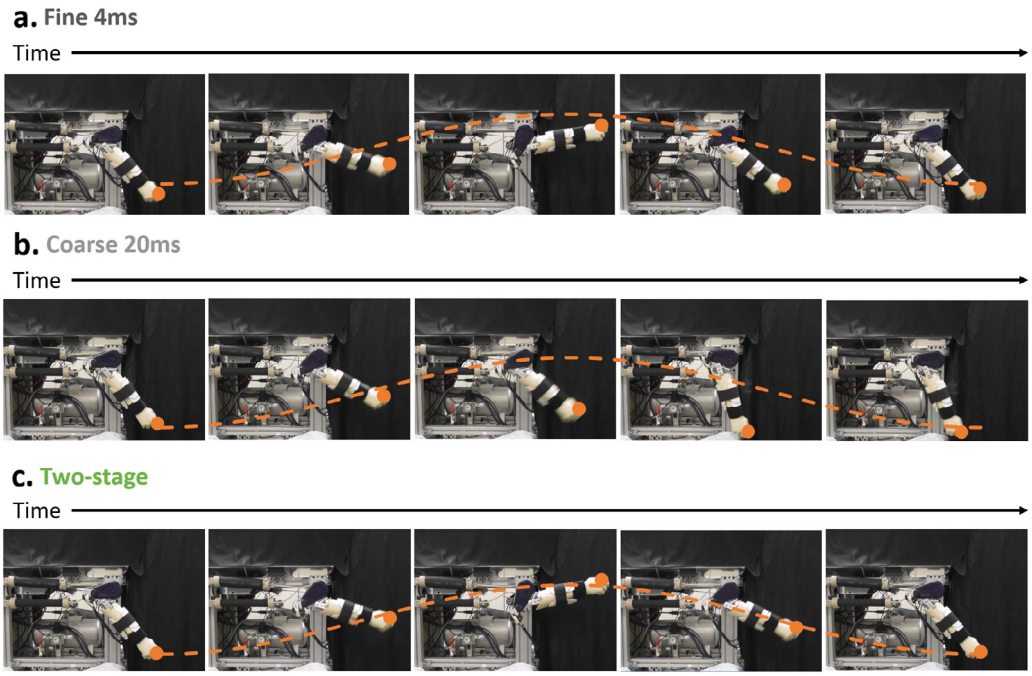

Fig. 7. Snapshots of generated motions of our forearm robot for target trajectory of 1.0 Hz using three optimal control strategies. Target trajectories are depicted on snapshots by dashed orange lines. (a), (b) for *Fine 4ms* and *Coarse 20ms* strategies, generated joint motions significantly deviated from target movements and failed to recover from failure situations after large deviations. (c) motions generated by proposed method successfully followed target trajectory without any large tracking errors.

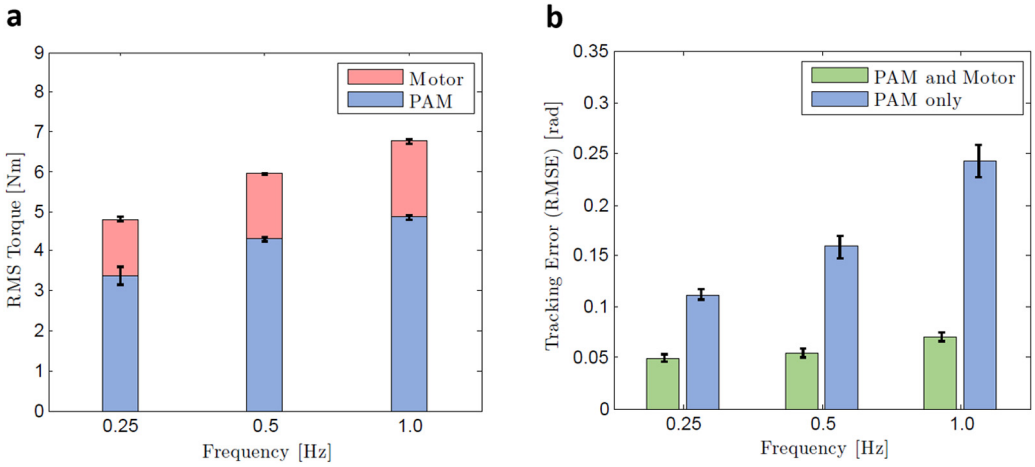

Fig. 8. Torque distribution: (a) contributions of each actuator to generate joint torques. Contribution of electric motor was much small than that of PAM in terms of amount of generated torque; (b) tracking errors of proposed hybrid control method and PAM-only approach. Results clearly indicated that electric motor greatly improved tracking performances, even though amount of output torque was much smaller than that of PAM.

of five experimental trials each of the proposed hybrid control method and the PAM-only approach. Error bars are standard deviations. The electric motor greatly improved the tracking performances although the amount of output torque was much smaller than that of PAM. Therefore, using multiple actuators to control a joint movement through real-time optimal control methods seems promising. Fig. 9 depicts the generated joint torque profiles to show how the torque was distributed to each actuator for the target sinusoidal trajectories of 0.25- and 1.0-Hz frequencies. For both target frequencies, the PAM and the electric motor were cooperatively activated for the target tracking tasks. The role of each actuator was dynamically changed according to the frequency of the target trajectory. The electric motor showed its peak torque earlier than the PAM to generate the upward movements at each cycle of the target trajectory with 1.0-Hz frequency. The quicker torque response of the electric motor successfully compensated the slower PAM movement.

6. Conclusion

We applied our proposed optimal control approach to derive a torque distribution strategy for our hybrid actuation system that is composed of a pneumatic artificial muscle and small and lightweight electric motors. We derived a singularly perturbed system to extract the fast dynamics for a forearm robot with a hybrid actuator. This property resembles the human muscle system, which is also composed of muscle fibers that have different twitch speeds (Burdet et al., 2013).

Optimal control methods are getting much attention as control algorithms for a wide variety of robots due to the recent rapid improvement of powerful computational resources (Kajita et al., 2003; Kuindersma et al., 2016; Mitrovic, Nagashima, Klanke, Matsubara, & Vijayakumar, 2010; Morimoto, Zeglin, & Atkeson, 2003; Stephens & Atkeson, 2010). However, a standard optimal control framework that can be applied to nonlinear systems only

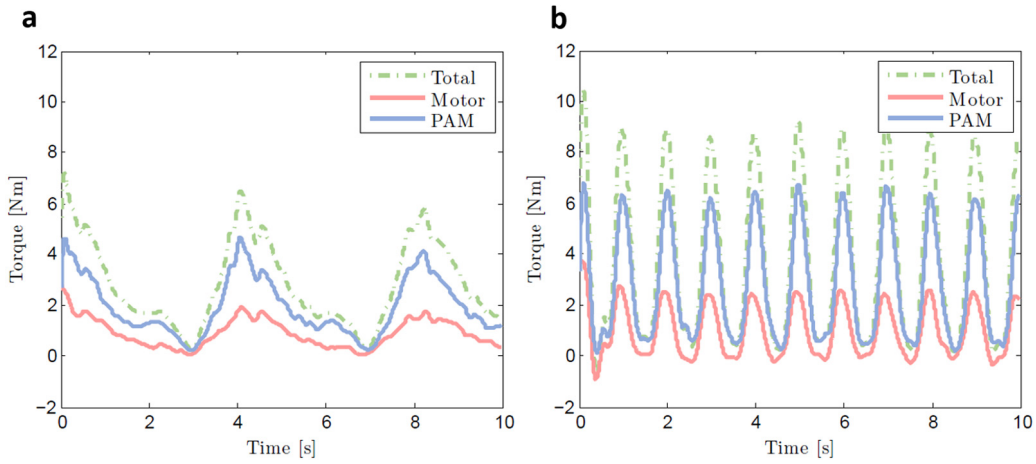

Fig. 9. Generated joint torque profiles to present how torque was dynamically distributed to each actuator for target sinusoidal trajectories of 0.25- and 1.0-Hz frequencies. For both target frequencies, PAM and electric motor were cooperatively activated for target tracking tasks. Moreover, the electric motor sometimes acted like antagonistic muscle in both cases for precise tracking by properly generating force to opposite direction of force generated by PAM.

provides an optimized control sequence that is calculated in an offline manner. Since such a pre-designed control sequence is susceptible to external disturbances, these standard offline optimal control approaches are not directly applicable for robot control in real environments. On the other hand, an online optimal control approach, also known as Model Predictive Control (MPC), can be useful since it updates an optimal control sequence at each control time step based on the current situation and can cope with the external disturbances influencing a robot (Seguchi & Ohtsuka, 2003; Wang, van Asseldonk, & van der Kooij, 2011). Moreover, MPC can derive control policies under a situation in which robots need to generate motions adaptively with changing objectives, e.g., dynamically changing the location of a target object or a target motion indicated by a human (Erez et al., 2013; Kumar, Tassa, Erez, & Todorov, 2014).

In our study, we proposed a two-stage optimal control strategy to reduce MPC's computational burden. We first derived the optimal control sequence for the original dynamics with coarse-time resolution and then optimized the short-term control sequence for the fast dynamical component with fine-time resolution. Since the extracted fast dynamical component of the forearm robot has lower-dimensional state space with lower-dimensional input, its computational burden was further reduced. Although application of the two-stage MPC was previously explored on a simulated chemical plant model (Chen et al., 2012) and a simulated biped model (Ishihara & Morimoto, 2015), in this study, we newly derived a singularly perturbed system for a hybrid actuator. To the best of our knowledge, ours is the first scheme that applied the two-stage MPC method to a real system and achieved successful results. As we presented in the experimental results, the computation time of the proposed approach was reduced much more than the required calculation time for solving the original optimal control problem. In our proposed two-stage MPC approach, after computing the optimal input voltages for the pneumatic actuator and the electric motor with coarse-time resolution, only the optimal sequence of the input voltages for the electric motor is re-optimized with fine-time resolution on fast dynamics. Thus, the proposed method successfully tracked the target trajectories in real-time without deterioration of the control performances (Figs. 3 and 4).

We empirically found that our proposed approach with properly selected time step sizes and horizons was able to generate stable control performance of the real hybrid actuation system. On the other hand, Lyapunov-based analyses for theoretically stable MPC have been studied (Jadbabaie, Yu, & Hauser, 2001; Mhaskar, El-Farra, & Christofides, 2006). Similarly, theoretical consideration about the stability for the two-stage MPC can be an important future research topic. Furthermore, future work will apply our proposed method to an exoskeleton robot with hybrid actuators (Hyon et al., 2011; Noda et al., 2012; Ugurlu et al., 2016). Moreover, since the dynamics of a biped robot can be transformed into a singularly perturbed system (Arimoto & Miyazaki, 1980; Ishihara & Morimoto, 2015), we might study a hierarchically combined singularly perturbed system for a bipedal exoskeleton robot with a hybrid actuator system.

Acknowledgments

This work was supported by JSPS Grant-in-Aid for JSPS Fellows 15J10675. Part of this research was supported by JSPS KAKENHI JP16H06565. It was also partially supported by MIC-SCOPE131207012, the project commissioned by the New Energy and Industrial Technology Development Organization (NEDO), SRPBS from AMED, "Development of Medical Devices and Systems for Advanced Medical Services" from NEDO/AMED, and ImPACT Program of Council for Science, Technology and Innovation (Cabinet Office, Government of Japan).

References

Ansari, A., Atkeson, C. G., Choset, H., & Travers, M. (2015). A survey of current exoskeletons and their control architectures and algorithms (draft 4.0), http://www.cs.cmu.edu/~cga/exo/survey.pdf.

Arimoto, S., & Miyazaki, F. (1980). A control theoretic study on dynamical biped locomotion. *Journal of Dynamic Systems, Measurement and Control, Transactions of the ASME*, *102*, 233–239.

Braun, D., Howard, M., & Vijayakumar, S. (2012). Optimal variable stiffness control: formulation and application to explosive movement tasks. *Autonomous Robots*, *33*(3), 237–253.

Burdet, E., Franklin, D. W., & Milner, T. E. (2013). *Human robotics: neuromechanics and motor control*. MIT Press.

Chen, X., Heidarinejad, M., Liu, J., & Christofides, P. D. (2012). Composite fast-slow mpc design for nonlinear singularly perturbed systems. *AIChE Journal*, *58*(6), 1802–1811.

Defense Advanced Research Projects Agency, (2015). Darpa robotics challenge finals home http://www.theroboticschallenge.org/.

Erez, T., Lowrey, K., Tassa, Y., Kumar, V., Kolev, S., & Todorov, E. (2013). An integrated system for real-time model predictive control of humanoid robots. In *2013 13th IEEE-RAS International conference on humanoid robots (Humanoids)* (pp. 292–299). IEEE.

Haddadin, S., Weis, M., Wolf, S., & Albu-Schäffer, A. (2011). Optimal control for maximizing link velocity of robotic variable stiffness joints. *IFAC Proceedings Volumes*, *44*(1), 6863–6871.

Hyon, S.-H., Morimoto, J., Matsubara, T., Noda, T., & Kawato, M. (2011). Xor: Hybrid drive exoskeleton robot that can balance. In *2011 IEEE/RSJ International conference on intelligent robots and systems* (pp. 3975–3981). IEEE.

Ishihara, K., & Morimoto, J. (2015). Real-time model predictive control with two-step optimization based on singularly perturbed system. In *2015 IEEE-RAS 15th International conference on humanoid robots (Humanoids)* (pp. 173–180). IEEE.

Jacobson, D. H. (1968). New second-order and first-order algorithms for determining optimal control: A differential dynamic programming approach. *Journal of Optimization Theory and Applications*, *2*(6), 411–440.

Jadbabaie, A., Yu, J., & Hauser, J. (2001). Unconstrained receding-horizon control of nonlinear systems. *IEEE Transactions on Automatic Control*, *46*(5), 776–783.

Kajita, S., Kanehiro, F., Kaneko, K., Fujiwara, K., Harada, K., Yokoi, K., et al. (2003). Biped walking pattern generation by using preview control of zero-moment point. In *IEEE International conference on robotics and automation, 2003. Proceedings, Vol. 2* (pp. 1620–1626). IEEE.

Kokotovic, P., Khalil, H. K., & O'reilly, J. (1999). *Singular perturbation methods in control: analysis and design, Vol. 25*. Siam.

Kuindersma, S., Deits, R., Fallon, M., Valenzuela, A., Dai, H., Permenter, F., et al. (2016). Optimization-based locomotion planning, estimation, and control design for the atlas humanoid robot. *Autonomous Robots*, *40*(3), 429–455.

Kumar, V., Tassa, Y., Erez, T., & Todorov, E. (2014). Real-time behaviour synthesis for dynamic hand-manipulation. In *2014 IEEE International conference on robotics and automation* (pp. 6808–6815). IEEE.

Lagerstrom, P., & Casten, R. (1972). Basic concepts underlying singular perturbation techniques. *Siam Review*, *14*(1), 63–120.

Makkar, C., Dixon, W., Sawyer, W., & Hu, G. (2005). A new continuously differentiable friction model for control systems design. In *2005 IEEE/ASME International conference on advanced intelligent mechatronics. Proceedings* (pp. 600–605). IEEE.

Matsubara, T., Noda, T., Hyon, S.-H., & Morimoto, J. (2011). An optimal control approach for hybrid actuator system. In *2011 11th IEEE-RAS International conference on humanoid robots (Humanoids)* (pp. 300–305). IEEE.

Mhaskar, P., El-Farra, N. H., & Christofides, P. D. (2006). Stabilization of nonlinear systems with state and control constraints using Lyapunov-based predictive control. *Systems & Control Letters*, *55*(8), 650–659.

Mitrovic, D., Nagashima, S., Klanke, S., Matsubara, T., & Vijayakumar, S. (2010). Optimal feedback control for anthropomorphic manipulators. In *2010 IEEE International conference on robotics and automation* (pp. 4143–4150). IEEE.

Morimoto, J., Zeglin, G., & Atkeson, C. G. (2003). Minimax differential dynamic programming: Application to a biped walking robot. In *2003 IEEE/RSJ International conference on intelligent robots and systems, 2003. (IROS 2003). Proceedings, Vol. 2* (pp. 1927–1932). IEEE.

Naidu, D. (2002). Singular perturbations and time scales in control theory and applications: an overview. *Dynamics of Continuous Discrete and Impulsive Systems Series B*, *9*, 233–278.

Noda, T., Sugimoto, N., Furukawa, J., Sato, M.-a., Hyon, S.-H., & Morimoto, J. (2012). Brain-controlled exoskeleton robot for bmi rehabilitation. In *2012 12th IEEE-RAS International conference on humanoid robots (Humanoids)* (pp. 21–27). IEEE.

Noda, T., Teramae, T., Ugurlu, B., & Morimoto, J. (2014). Development of an upper limb exoskeleton powered via pneumatic electric hybrid actuators with bowden cable. In *2014 IEEE/RSJ International conference on intelligent robots and systems* (pp. 3573–3578). IEEE.

OpenMP ARB OpenMP, http://www.openmp.org/.

Qin, S. J., & Badgwell, T. A. (1997). An overview of industrial model predictive control technology. *AIChE Symposium Series*, *93*(316), 232–256.

Sardellitti, I., Park, J., Shin, D., & Khatib, O. (2007). Air muscle controller design in the distributed macro-mini (dm 2) actuation approach. In *IEEE/RSJ International conference on intelligent robots and systems, 2007* (pp. 1822–1827). IEEE.

Seguchi, H., & Ohtsuka, T. (2003). Nonlinear receding horizon control of an underactuated hovercraft. *International Journal of Robust and Nonlinear Control*, *13*(3–4), 381–398.

Siciliano, B., & Book, W. J. (1988). A singular perturbation approach to control of lightweight flexible manipulators. *International Journal of Robotics Research*, *7*(4), 79–90.

Stephens, B. J., & Atkeson, C. G. (2010). Push recovery by stepping for humanoid robots with force controlled joints. In *2010 10th IEEE-RAS International conference on humanoid robots* (pp. 52–59). IEEE.

Teramae, T., Noda, T., & Morimoto, J. (2014). Optimal control approach for pneumatic artificial muscle with using pressure-force conversion model. In *2014 IEEE International conference on robotics and automation* (pp. 4792–4797). IEEE.

Todorov, E., & Li, W. (2005). A generalized iterative lqg method for locally-optimal feedback control of constrained nonlinear stochastic systems. In *Proceedings of the 2005, American control conference, 2005.* (pp. 300–306). IEEE.

Ugurlu, B., Doppmann, C., Hamaya, M., Forni, P., Teramae, T., Noda, T., et al. (2016). Variable ankle stiffness improves balance control: experiments on a bipedal exoskeleton. *IEEE/ASME Transactions on Mechatronics*, *21*(1), 79–87.

Van Dyke, M. (1975). *Perturbation methods in fluid mechanics*. Parabolic Press, Incorporated.

Wang, L., van Asseldonk, E. H., & van der Kooij, H. (2011). Model predictive control-based gait pattern generation for wearable exoskeletons. In *2011 IEEE International conference on rehabilitation robotics* (pp. 1–6). IEEE.